Eur. Phys. J. B **32**, 471–476 (2003)
DOI: 10.1140/epjb/e2003-00128-1

THE EUROPEAN PHYSICAL JOURNAL B

# Epitaxial growth and magnetic and electric properties of Co-doped $TiO_2$ thin films

## Is nonequilibrium doping an essential for ferromagnetism?

J. Li[1,a], C.H. Sow[2], X.S. Rao[3], C.K. Ong[2], and D.N. Zheng[1]

[1] Institute of Physics, Chinese Academy of Sciences, Beijing 100080, PR China
[2] Centre for Superconducting and Magnetic Materials and Department of Physics, National University of Singapore, 2 Science Drive 3, Singapore 117542
[3] Temasek Laboratories, Engineering Drive 3, 10 Kent Ridge Crescent, Singapore 119260

Received 8 January 2003 / Received in final form 7 March 2003
Published online 7 May 2003 – 

**Abstract.** In this research, *c*-axis oriented epitaxial anatase $TiO_2$ thin films were grown on $SrTiO_3(100)$ substrates using a ceramic $Ti_{0.95}Co_{0.05}O_2$ target by Pulsed Laser Deposition (PLD). The film growth processes were monitored by reflective high energy electronic diffraction (RHEED). Microstructure, conductivity, and magnetism of these doped films are found strongly affected by the oxygen pressure and substrate temperature $T_s$. Grown at a $T_s$ around 750 °C in an oxygen pressure of 0.2 mbar, the dopants are found existing as oxide inclusions. The doped film thus behaves as an insulator and shows diamagnetism in a magnetic field parallel to the film surface. However, in the doped film grown at a reduced temperature of 630 °C in a vacuum, no impurity phase can be identified. The film shows a saturated magnetic moment of $0.16\mu_B$/Co and a fairly good conductivity at room temperature. It is then concluded that nonequilibrium growth at lower temperatures in vacuum is essential for a high solubility of Co in the $TiO_2$ lattice and thus the ferromagnetism.

**PACS.** 75.50.Pp Magnetic semiconductors – 81.15.Fg Laser deposition – 68.55.Jk Structure and morphology; thickness; crystalline orientation and texture – 61.14.Hg Low-energy electron diffraction (LEED) and reflection high-energy electron diffraction (RHEED)

## 1 Introduction

Titanium dioxide ($TiO_2$) is traditionally the most widely used white pigment due to its high refractive index. These years, $TiO_2$ has received considerable attentions. More and more applications have been developed. It has been used for optical coatings, photocatalysis agents, gas-sensors, and solar cells [1,2]. Its high-permittivity also makes it a promising candidate for the next generation gate insulators [3,4]. In addition it is found that high quality $TiO_2$ nanotubes can be readily fabricated [5,6]. Nevertheless, the most striking of all is the recent discovery of room-temperature ferromagnetism in the Co-doped anatase $TiO_2$ thin films [7,8]. This diluted magnetic oxides (DMO) based on $TiO_2$ presents not only ferromagnetism, but also transparency and conductivity matching with semiconductors, thus is expected to be a good spin injector for the newly established spintronics.

More recently, ferromagnetism was again reported by Chambers *et al.* in Co-doped anatase $TiO_2$ films grown by oxygen-plasma-assisted molecular beam epitaxy (MBE) [9,10]. They observed a saturated magnetic moment of $1.26\mu_B$/Co in their $Co_{0.03}Ti_{0.97}O_2$ film, larger than the value previously reported [7]. The magnetic moment was accounted for the unquenched orbital moment of Co(II) ions in the asymmetry crystal field. Meanwhile, a theoretical work on the electronic structure of the Co substituted $TiO_2$ also predicted a ferromagnetic ground state with a *half-metallic* nature [11]. This ferromagnetic state was pictured based on the double-exchange mechanism first proposed by Zener [12,13]. Later, ferromagnetism in Co-doped $TiO_2$ films, either of the anatase phase or the rutile phase, has been re-claimed by several other groups [14–16], although some researchers argued that dispersed cobalt nanoclusters are the origin of the ferromagnetism observed [16].

Relative to the extensive studies aimed to other applications, experimental data on the $TiO_2$-based DMO are still deficient, greatly growth-condition-dependent, and even controversial. Attentions have been attracted on the doping concentration and oxygen pressure during depositions. Ferromagnetism is only discovered in films

[a] e-mail: lijie@ssc.iphy.ac.cn

deposited at very low oxygen pressures, although no convincing explanation has been given. The deposition temperature $T_s$, however, has been constricted in a fairly narrow range due to the fact that anatase-to-rutile phase transition may occur as $T_s$ is raised [4]. In this experiment, we extended the temperature range from a moderate $T_s = 630$ °C to a fairly high $T_s = 750$ °C, where the solubility of cobalt in the lattice is different. Our result reveals that the ferromagnetism observed in the Co-doped $TiO_2$ films is due to the substituted Co ions in the lattice, instead of the dispersed cobalt clusters.

## 2 Experimental details

The cobalt doped $TiO_2$ films were deposited on (100)$SrTiO_3$ single crystal substrates by using a laser molecular-beam-epitaxy system (laser MBE) equipped with an *in situ* reflection high energy electronic diffraction (RHEED) accessory. Details concerning our systems have been reported elsewhere [17,18]. Ceramic $Ti_{0.95}Co_{0.05}O_2$ bulk of dimension $\Phi$30 mm × 4 mm was chosen as the target. The target was sintered using conventional solid state reaction technique at 1300 °C. X-ray diffraction (XRD) pattern of the target reveals a mixture of the rutile $TiO_2$ phase and another phase rich of Co. Details will be given in the next section. The chamber was first pumped to $2 \times 10^{-6}$ mbar. Prior to deposition, the substrates were heated up to 750–800 °C and kept for half an hour to let off the surface absorptions and relieve the stress caused by the previous mechanical polishing. The films were grown at a temperature ranging from 600–800 °C in either the background vacuum or a fixed oxygen pressure of 0.2 mbar. During the deposition, the energy density of the KrF eximer laser was 1.5 J/cm$^2$, and the frequency of laser pulse was 1 Hz. The growth rate, which is estimated to be around 0.1 nm/s, varied with the substrate temperature and the oxygen pressure during film deposition. As grown in vacuum, the film crystallinity were *in situ* monitored by RHEED with electron energy of 14–18 keV, and the images were recorded by a charge-coupled device (CCD) camera and analyzed with a computer. After deposition the films were cooled down to room temperature in 40 min without changing the ambience. Microstructure of the doped $TiO_2$ films were studied by XRD and atomic force microscopy (AFM), and the magnetic properties were characterized by a vibrating sample magnetometer (VSM).

## 3 Experimental results

### 3.1 Microstructure of the targets

Microstructure of the ceramic target $Ti_{0.95}Co_{0.05}O_2$ was studied by fine XRD scans prior to the film deposition. The spectrum is illustrated in Figure 1. Different from the case of pure $TiO_2$ bulk sintered under similar conditions [17], which shows a mixture of the anatase and the rutile phase, no trace of the anatase phase was identified in the Co-doped target. As a compensation, another phase rich of Co, $CoTi_2O_5$ ($CoO \cdot 2TiO_2$), was found. This impurity phase, which is dark-greenish-black itself, is also the origin of the green-grey color of the Co-doped target. Peak positions of this phase are labelled by $'\nabla'$ in the spectrum, indicating a tetragonal structure.

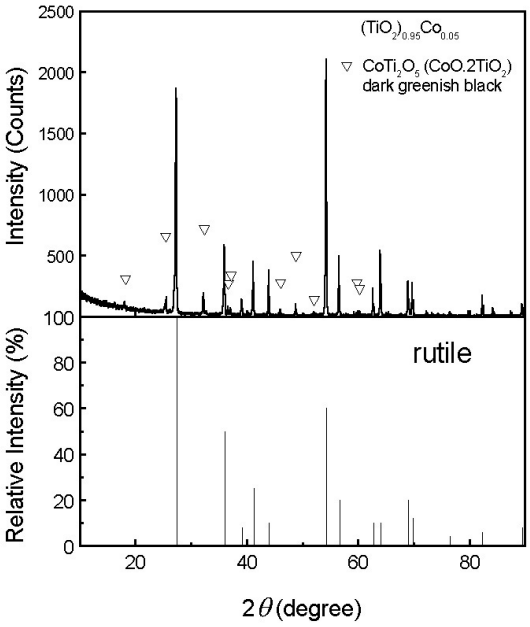


**Fig. 1.** The XRD spectrum of the cobalt doped target $Ti_{0.95}Co_{0.05}O_2$. Peak positions from the rutile $TiO_2$ phase are indicated in the bottom panel. Peaks attributed to the $CoTi_2O_5$ phase are labelled at the spectrum by ▽.

### 3.2 In situ RHEED observations

Most of the films grown in vacuum were monitored by real-time RHEED, and that grown in 0.2 mbar oxygen were also checked *in situ* by RHEED after the film deposition. The recorded diffraction patterns of the Co-doped $TiO_2$ film grown at $T_s = 750$ °C in vacuum are shown in Figure 2, labelled by *a* to *e* according to their time sequence. As shown in Figure 2a, the surface of the $SrTiO_3$ substrate is almost perfect, with diffraction spots arranged on a semi-circle, which are in fact the intersects of the reciprocal lattice with the Ewald sphere. Clear Kikuchi lines can be observed. Investigation shows that heating up the substrate to a temperature of 750 °C or higher and keeping for a certain period of time can further improve the substrate surface condition. After the first several laser pulses, a very thin layer of $TiO_2$ film seeded on the substrate. The reciprocal lattice of a 2-D film consists of streaks, which are tangential to the Ewald sphere, forming the pattern shown in Figure 2b. The sharply decreased diffraction intensity in this figure could be due to the very small thickness of the film. With increase of the deposition time and thus increase of the film thickness, intensity of the diffraction streaks recovered gradually, as shown in Figure 2c.

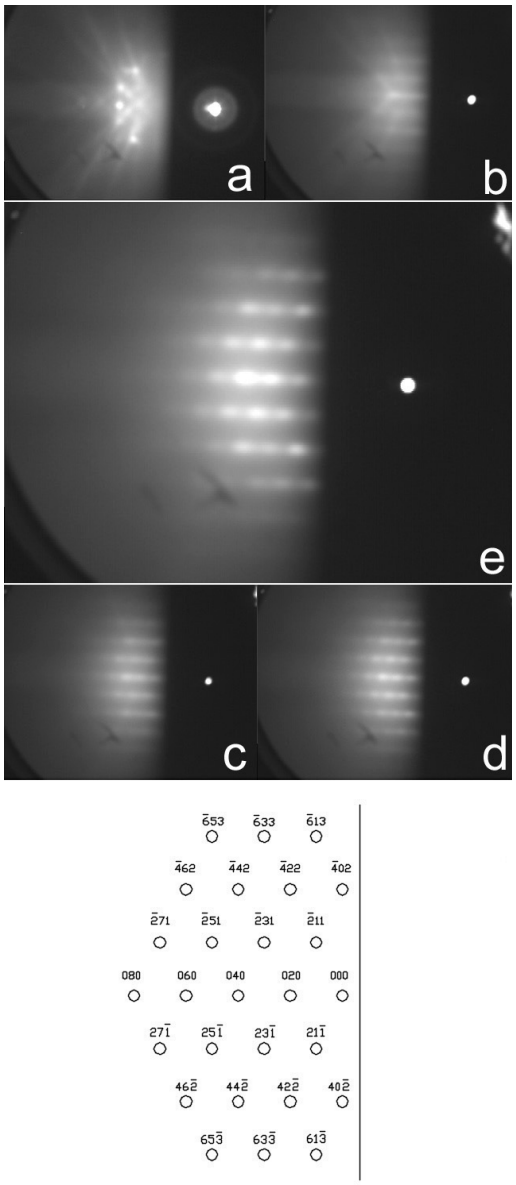


**Fig. 2.** RHEED patterns at different growth stages. (a) the single crystal $SrTiO_3$ substrate at room temperature. (b) the very initial growth stages of the $TiO_2$ film. (c) after deposited for one or two minutes. (d) after deposited for 18 minutes. (e) After the deposition lasted for 25 minutes; Bottom panel shows the indexing and simulation result. The zone axis is determined to be [102] of the $TiO_2$ anatase phase.

As the deposition further progressed, the RHEED pattern changed slowly from streaks to elongated spots or rods as in Figure 2d. It is clear that the figure resembles the electron diffraction pattern of a transmission electron microscopy (TEM) which reveals a reciprocal lattice of a 3-D crystal. Therefore Figure 2d is a sign that the electron beam has travelled through the ridges formed on the film surface. It indicates the gradually increased roughness on the film surface with the deposition time. Figure 2e shows the diffraction pattern recorded at the 25th minute. Even more roundish diffraction spots would be observed in the

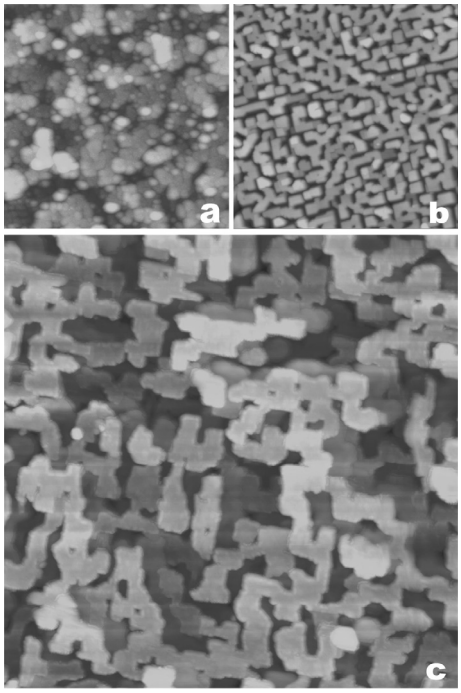


**Fig. 3.** AFM images for surface of (a) a Co-doped $TiO_2$ film deposited at $T_s = 750$ °C in vacuum (b) a Co-doped $TiO_2$ film deposited at $T_s = 750$ °C in 0.2 mbar $O_2$ (c) a Co-doped film deposited at $T_s = 630$ °C in vacuum. The scan scales for (a) and (b) are $1 \times 1$ $\mu m^2$, while that for (c) is $2 \times 2$ $\mu m^2$.

RHEED pattern if the deposition was further extended, and the intensity of the spots gradually decline, indicating a rougher film surface. No clear RHEED intensity oscillation or sign of the $(1 \times 4)$ surface re-construction has been observed during film deposition, perhaps due to the relatively large lattice mismatch between the anatase $TiO_2$ and the $SrTiO_3$ substrate [19–21].

The RHEED pattern shown in Figure 2e is analyzed and the zone axis is determined to be [102] of the anatase $TiO_2$, which suggested that the RHEED in our system is not well configurated and the incident electron beam is 11° away from the film surface. The pattern shown in the bottom panel of Figure 2 are simulation results using an electron microscopy image simulation (EMS) software. Figure 2 provides a solid evidence that the $TiO_2$ films grown are single crystal-like, which is not only epitaxial along the *c*-axis, but also aligns along the *ab* directions. Cobalt doping affects little the $TiO_2$ film crystal structure. RHEED observation for the films deposited at 750 °C in 0.2 mbar oxygen shows similar patterns but the round diffraction spots suggest a rougher film surface.

### 3.3 Morphology of the film surface

The film topography was carefully investigated by AFM and the images obtained are shown in Figure 3. The Co-doped film grown in a background vacuum of $2 \times 10^{-6}$ mbar, as presented in Figure 3a, shows irregular or sphere-like grains. As the oxygen pressure during film

deposition increased to 0.2 mbar, the grain shape becomes regular, as presented in Figure 3b. The film exhibits corner-connected rectangular-shaped grains with width of 40 $\sim$ 50 nm and length ranging from 60 to 150 nm. The cube-to-cube in-plane orientation nature is clearly revealed, consisting with the RHEED observations. Scan scales for the two figures are $1\times1$ $\mu$m$^2$. The Co-doped film grown at a lower $T_s$ of 630 °C in the background vacuum is also shown in Figure 3c, which consists of grains with similar shape as Figure 3b, but with remarkably enlarged grain size. To convenient size comparison, the scan scale for this figure is $2\times2$ $\mu$m$^2$. The $z$ scale of all the figures shown is less than 50 nm, suggesting a relatively smooth film surface.

The different grain shape presented in Figure 3a may be due to the electron beam irradiation during the film deposition, because the whole growth process for this film was monitored by RHEED. Comparing Figures 3b and c, one can conclude that the deposition ambience actually does not affect the grain shape of the films much, although the film deposited at 630 °C has a larger grain size, which is against intuition. It is then suggested that, at higher $T_s$, where the solubility of cobalt in the lattice is limited, the impurity may diffuse to grain boundaries and accumulate there forming clusters, which hampers the $TiO_2$ grain growth. Additional evidence was provided by the Fe-doped $TiO_2$ film (AFM image not shown) grown at same conditions as Figure 3b, which consists of tabular grains of similar size $20\times60$ nm$^2$. Most of these grains align with their longitude along only one axis of the substrate. It is then obvious that the doping remarkably changes the grain shape. Generally, grain shape of a certain crystal, if free of absorption, is only determined by the energy for different crystal surfaces [22]. Therefore a change in grain shape must be resulted from a change of the relative surface energies due to the existence of impurity particles at the grain boundaries.

### 3.4 Microstructure of the films

The microstructure of all the as-deposited films were examined by XRD, and the typical $\theta-2\theta$ spectra are presented in Figure 4. Grown at 750 °C in 0.2 mbar oxygen, the film shows only (004) and (008) peaks of the anatase phase, as seen in the bottom curve in Figure 4, indicating its complete $c$-axis orientation. It is noted that the intensity of peak (004) is not quite high, due to the relatively low structure factor $F_{004}$. The lattice constant is determined to be 9.52 Å, comparable to the undoped bulk value 9.514 Å from the ICDD database. The full width at half maximum (FWHM) of the $TiO_2$ (004) rocking curve, as shown in the right-hand inset in Figure 4, is around 1.0° before the instrumental broadening is excluded. Obviously, although the RHEED patterns suggest a single-crystal-like structure of the film, its crystallinity is still poor due to the large lattice mismatch between the film and the substrate [21]. In spite of the fact that the film shows very good transparency, an impurity phase has been identified to be $TiCo_2O_5$, same as that in the bulk target.

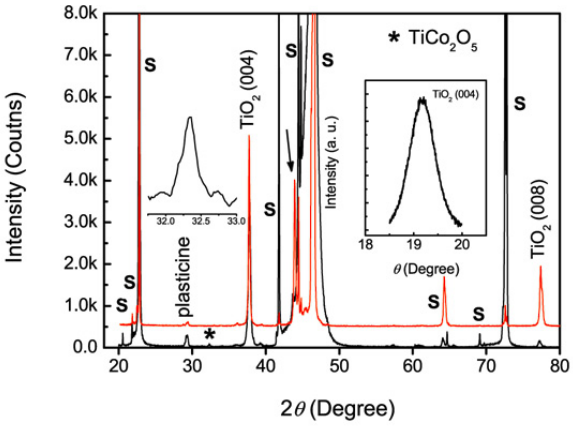


**Fig. 4.** XRD spectra for the Co-doped $TiO_2$ films deposited at 630 °C in vacuum (top) and at 750 °C in an oxygen pressure of 0.2 mbar (bottom). Reflections attributed to the (004) and (008) of anatase $TiO_2$ are observed. Peaks labelled by '$S$' are due to the $SrTiO_3$(100) substrate. The left inset shows reflection (230) of the impurity phase $TiCo_2O_5$, appearing around 32.3°, as labelled by '$\star$' in the bottom spectrum. The right inset is the $\Omega$ scan of the $TiO_2$ (004) for the bottom spectrum.

The left inset in Figure 4 shows its (230) peak, which centers at 32.33°, as labelled by '$S$' in the spectrum. On the contrary, grown at the same $T_s$ in vacuum, no impurity peak besides the anatase (00$l$) appears in the film spectrum, although the cobalt dopants may exist as a metal phase, whose peak can be masked by the $SrTiO_3$(100) reflections. Therefore grown at 750 °C, at least in a high oxygen pressure, due to the low solubility of cobalt in the lattice, the dopant may exist only in a form of impurity phase.

While all the films grown at 750 °C are colorless and transparent, the film grown at a lower $T_s$ of 630 °C in vacuum is transparent but shows clear green color. Its XRD spectrum, as can be seen in the top curve in Figure 4, shows not only the (004) and (008) peaks of the anatase phase, but also the (210) of the rutile phase at 43.94°, as indicated by a black arrow in Figure 4. Rutile phase with this orientation may also epitaxy on the substrate with 45 degree in-plane rotation. The lattice mismatch along the two perpendicular directions are $\pm7\%$ respectively. A slit extension of the rutile out-of-plane lattice has been detected, while no obvious parameter change happens in the anatase phase. No impurity peak has been observed. Therefore the XRD data imply that the cobalt dopants may substitute into the lattice of the rutile phase in this sample, due to the higher nonequilibrium solubility at this $T_s$. We aware that the observation is odd in some extend, since the rutile phase is used to being connected to a higher temperature.

### 3.5 Electrical and magnetic properties of the films

None of the films deposited at $T_s = 750$ °C, either in vacuum or in 0.2 mbar oxygen, is electrical conducting. Their

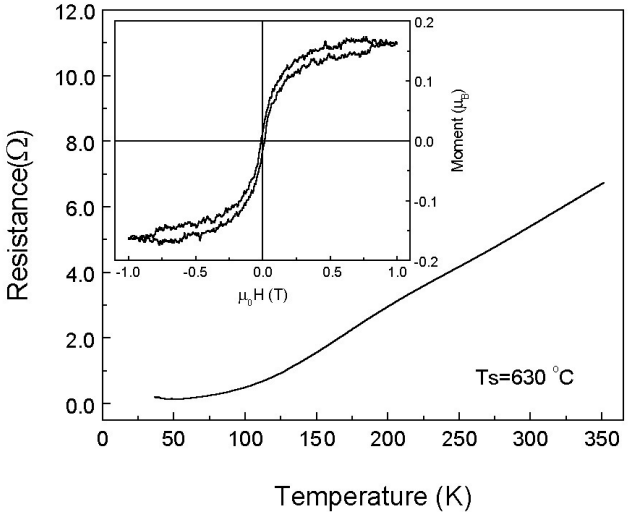


**Fig. 5.** *R-T* curve for the Co-doped $TiO_2$ film deposited at 630 °C in vacuum. Inset shows the *M vs. H* curve of the film. The applied magnetic field was parallel to the film surface.

room temperature resistance all exceeds 100 MΩ. On the contrary, the film deposited at $T_s$ = 630 °C in vacuum is a good conductor. The *R-T* curve of this film is shown in Figure 5. As cooling down, its resistance decreases linearly with temperature, while a deviation occurs at 220 K. This deviation may suggest a structure change in the film, which needs to be studied further. As temperature reaches 50 K, the curve finds its minimum. An insulating behavior is expected as temperature is further reduced, although it is beyond the scope of our instrument. It is then conclude that, at low temperature region, the conducting mechanism is thermal activation; while at higher temperatures, when all the carriers are activated, the dominant conducting mechanism becomes the carrier-scattering by the lattice.

Accordingly, none of the films deposited at $T_s$ = 750 °C shows ferromagnetism. Instead, the films are diamagnetic in a parallel magnetic field with comparable negative magnetic moments. It suggests that this is only the magnetic behavior of pure anatase $TiO_2$, while Co doping in these films has no effect. Here it is noted that, even for the films deposited at 750 °C in vacuum, where the cobalt impurity most probably exists as metallic clusters or CoO, no ferromagnetism has been observed. The reason behind this observation, which is different from the previous reports, should be the fact that Co does not substituted into the $TiO_2$ lattice in these films, instead it exists as a second phase at grain boundaries. However, as shown in the inset of Figure 5, the film deposited at $T_s$ = 630 °C in vacuum shows a saturated magnetic moment of 0.16$\mu$B/Co in a magnetic field parallel to the film surface, although its coercivity cannot be accurately determined by VSM. In this figure, the diamagnetic background of the $SrTiO_3$ substrate has been carefully removed. We attribute the ferromagnetism observed to the substituted cobalt ions in the lattice due to the enhanced solubility during the nonequilibrium growth.

## 4 Discussions

Theoretical calculations [11,13] predicted a ferromagnetic ground state in the Co-doped $TiO_2$ by assuming that Co ions substitute the Ti-cations in the lattice. The ferromagnetism is argued to be the carrier-induced type, which should be accompanied by a metallic transport behavior.

We demonstrated, however, the equilibrium solubility of cobalt ions in the anatase $TiO_2$ lattice is quite limited. During the solid state reaction process of the target, a chemical equilibrium has been well established. The most stable form of Co in the $TiO_2$ target is the $CoO \cdot 2TiO_2$, which is evaporated as molecules onto the substrate during the film deposition, providing enough oxygen is supplied. The impurity accumulates at grain boundaries. Since the magnetic moment of CoO is only about 0.01$\mu_B$/site [23], no ferromagnetism can be observed in the films. While depositing in vacuum, although $CoO \cdot 2TiO_2$ is partially deoxidized, it still exists in the film as an impurity if only $T_s$ is high enough, so the film still shows no ferromagnetism and accordingly no electrical conduction.

Just as in the case of diluted magnetic III-V semiconductor [24], low solubility of cobalt in the $TiO_2$ lattice can be overcome by low-temperature nonequilibrium growth, as in our experiment the film growth at a $T_s$ = 630 °C in vacuum. The Co ions can be substituted directly into the $TiO_2$ lattice. In this sense, the molecular beam epitaxy (MBE) is a better technique to grow Co-doped ferromagnetic $TiO_2$, since it allows to work far from equilibrium. This may also be the reason that the films prepared by Chambers *et al.* show a higher magnetic moment [9,10]. Our experimental result suggests that the nonequilibrium solubility of Co in the rutile phase is higher. Matsumoto's also claimed a fairly high magnetic moment in the rutile phase in his recent paper [25]. Further experiments are necessary.

## 5 Conclusions

In summary, high quality Co-doped anatase (001)$TiO_2$ films have been grown on (100)$SrTiO_3$ substrates. As $T_s$ is high enough, the dopants have been found existing as impurity phases near grain boundaries and affecting only the grain shape. No ferromagnetism has been observed. As $T_s$ is reduced, due to the nonequilibrium growth, the solubility of cobalt in the $TiO_2$ lattice, most probably in the rutile phase, increases and thus the film shows ferromagnetism and a metallic conducting behavior.

## References

1. G.H. Li, L. Yang, Y.X. Jin, L.D. Zhang, Thin Solid Films **368**, 163 (2000)
2. M. Thelakkat, C. Schmitz, H.-W. Schmidt, Adv. Mater. **14**, 577 (2002)
3. K. Fukushima, I. Yamada, J. Appl. Phys. **65**, 619 (1988)
4. S.A. Campbell, H.-S. Kim, D.C. Gilmer, B. He, T. Ma, W.L. Gladfelter, IBM J. Res. Develop. **43**, 383 (1999)

5. G.H. Du, Q. Chen, R.C. Che, Z.Y. Yuan, L.-M. Peng, Appl. Phys. Lett. **79**, 3702 (2001)
6. D.W. Gong, C.A. Grimes, O.K. Varghese, W.C. Hu, R.S. Singh, Z. Chen, E.C. Dickey, J. Mater. Res. **16**, 3331 (2001)
7. Y. Matsumoto, M. Murakami, T. Shono, T. Hasegawa, T. Fukumura, M. Kawasaki, P. Ahmet, T. Chikyow, S.-Y. Koshihara, H. Koinuma, Science **291**, 854 (2001)
8. Y. Matsumoto, M. Murakami, T. Hasegawa, T. Fukumura, M. Kawasaki, P. Ahmet, K. Nakajima, T. Chikyow, H. Koinuma, Appl. Surf. Sci. **189**, 344 (2002)
9. S.A. Chambers, S. Thevuthasan, R.F.C. Farrow, R.F. Marks, J.U. Thiele, L. Folks, M.G. Samant, A.J. Kellock, N. Ruzycki, D.L. Ederer, U. Diebold, Appl. Phys. Lett. **79**, 3467 (2001)
10. S.A. Chambers, C.M. Wang, S. Thevuthasan, T. Droubay, D.E. McCready, A.S. Lea, V. Shutthanandan, C.F. Windisch Jr, Thin Solid Films **418**, 197 (2002)
11. M.S. Park, S.K. Kwon, B.I. Min, Phys. Rev. B **65**, 161201 (2002)
12. C. Zener, Phys. Rev. **82**, 403 (1951)
13. T. Dietl, H. Ohno, F. Matsukura, J. Cibert, D. Ferrand, Science **287**, 1019 (2000)
14. In-Bo Shim, Sung-Yong An, Chul Sung Kim, Se-Young Choi, Yong Wook Park, J. Appl. Phys. **91**, 7914 (2002)
15. Wan Kyu Park, R.J. Ortega-Hertogs, J.S. Moodera, A. Punnoose, M.S. Seehra, J. Appl. Phys. **91**, 8093 (2002)
16. D.H. Kim, J.S. Yang, K.W. Lee, S.D. Bu, T.W. Noh, S.-J. Oh, Y.-W. Kim, J.-S. Chung, H. Tanaka, H.Y. Lee, T. Kawai, Appl. Phys. Lett. **81**, 2421 (2002)
17. C.K. Ong, S.J. Wang, Appl. Surf. Sci. **185**, 47 (2001)
18. P. Chen, S.Y. Xu, W.Z. Zhou, C.K. Ong, D.F. Cui, J. Appl. Phys. Lett. **85**, 3000 (1999)
19. Y. Liang, S. Gan, S. A. Chambers, E.I. Altman, Phys. Rev. B **63**, 235402 (2001)
20. G.S. Herman, M.R. Sievers, Y. Gao, Phys. Rev. Lett. **84**, 3354 (2000)
21. M. Murakami, Y. Matsumoto, K. Nakajima, T. Makino, Y. Segawa, T. Chikyow, P. Ahmet, M. Kawasaki, H. Koinuma, Appl. Phys. Lett. **78**, 2664 (2001)
22. A. Beltrán, J.R. Sambrano, M. Calatayud, F.R. Sensato, J. Andrés, Surf. Sci. **490**, 116 (2001)
23. K. Ueda, H. Tabata, T. Kawai, Appl. Phys. Lett. **79**, 988 (2001)
24. H. Ohno, Science **281**, 951 (1998)
25. Y. Matsumoto, R. Takahashi, M. Murakami, T. Koida, X.J. Fan, T. Hasegawa, T. Fukumura, M. Kawasaki, S.Y. Koshihara, H. Koinuma, Jpn J. Appl. Phys. **40**, L1204 (2001)